BIOCHEMISTRY

 Volume 45, Number 48 December 5, 2006

Current Topics

Calmodulin, Conformational States, and Calcium Signaling. A Single-Molecule Perspective†

Carey K. Johnson‡

Department of Chemistry, 1251 Wescoe Drive, University of Kansas, Lawrence, Kansas 66045-7582

Received May 27, 2006; Revised Manuscript Received September 30, 2006

ABSTRACT: Single-molecule fluorescence measurements can provide a new perspective on the conformations, dynamics, and interactions of proteins. Recent examples are described illustrating the application of single-molecule fluorescence spectroscopy to calcium signaling proteins with an emphasis on the new information available in single-molecule fluorescence burst measurements, resonance energy transfer, and polarization modulation methods. Calcium signaling pathways are crucial in many cellular processes. The calcium binding protein calmodulin (CaM) serves as a molecular switch to regulate a network of calcium signaling pathways. Single-molecule spectroscopic methods can yield insights into conformations and dynamics of CaM and CaM-regulated proteins. Examples include studies of the conformations and dynamics of CaM, binding of target peptides, and interaction with the plasma-membrane Ca^{2+} pump. Single-molecule resonance energy transfer measurements revealed conformational substates of CaM, and single-molecule polarization modulation spectroscopy was used to probe interactions between CaM and the plasma-membrane Ca^{2+}-ATPase.

Single-molecule fluorescence methods have the potential to resolve details about protein conformations, interactions, and dynamics that were previously hidden by ensemble averaging. As the practice of single-molecule methods expands, it is useful to examine what new information can be obtained about biomolecules and what the limitations of the methods are. This paper will examine these questions in the context of recent applications of single-molecule fluorescence techniques in the author's laboratory to the conformations, dynamics, and interactions of the calcium signaling protein calmodulin (CaM[1]) (see Figure 1).

Proteins are dynamic molecules. Multiple conformational states are required for them to function. CaM is no exception and appears to sample an unusually wide range of conformations (*1*). How can the distribution of such conformations be characterized? Conventional bulk measurements detect the average properties of many (typically $>10^{10}$) molecules and therefore do not resolve the range of conformations that are actually present. One way to attack this problem is to detect and characterize molecules one at a time.

Introduced in the early 1990s (*2*−*6*), single-molecule fluorescence methods can now address real problems in biology (see recent reviews (*7*−*10*)). Conformational states and conformational motions can be detected that may be

† I acknowledge support for this research from NIH R01 GM58715, the American Heart Association (99513262 and 0455487Z), and a Research Corporation Research Opportunity Award.

‡ E-mail: ckjohnson@ku.edu.

[1] Abbreviations: AF488, Alexa Fluor 488 maleimide; APD, avalanche photodiode; CaM, calmodulin; CaM-DA, a CaM mutant with cysteine substituted at sites 34 and 110 and doubly-labeled with AF488 and TR; CCD, charge-coupled device; FRET, fluorescence resonance energy transfer; MBP, maltose binding protein; NOE, nuclear Overhauser effect; PMCA, plasma-membrane Ca^{2+}-ATPase; TMR, tetramethylrhodamine; TR, Texas Red maleimide.

10.1021/bi061058e CCC: $33.50
Published on Web 11/09/2006

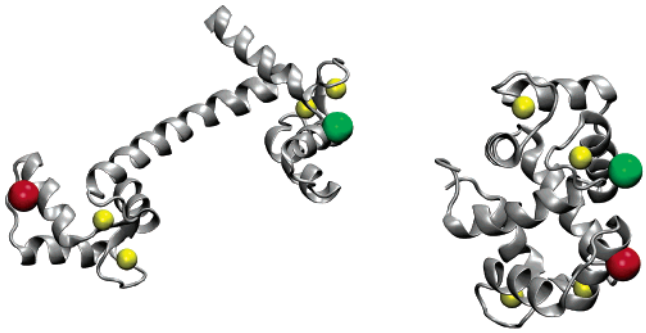

FIGURE 1: Crystal structures of Ca^{2+}-CaM showing labeling sites 34 and 110 (red and green spheres). The structure on the left shows CaM in an extended conformation with a helical central linker (pdb 3cln (*127*)). The structure on the right shows a compact conformation with a sharply bent central linker (pdb 1prw (*89*)). Figures were generated in VMD for WIN32, version 1.8.4 (*128*).

missed by other methods. Dynamic processes can be probed under either equilibrium or nonequilibrium conditions by following the fluctuations of an appropriate single-molecule spectroscopic signal. In kinetic measurements, the problem of temporal synchronization in ensemble experiments (e.g., by stop-flow, temperature jump, or flash photolysis) is circumvented, as there is a population of only one. Of course, other methods can also provide information on conformational heterogeneity, and single-molecule methods bring their own set of challenges. Nevertheless, in many biological systems, single-molecule fluorescence methods have produced new insights that complement more traditional structural and biochemical approaches.

The potentials and limitations of the methods used and the resulting information are described below in the context of our studies in CaM. In our laboratory we have applied single-molecule spectroscopy to CaM on three levels: (1) the structure and dynamics of CaM itself; (2) CaM binding to peptide targets representing CaM-binding domains of target enzymes; and (3) CaM binding and activation of a target enzyme, plasma-membrane Ca^{2+}-ATPase (PMCA). It is important to stress, however, that these are just examples among many applications of single-molecule methods to many areas of biology, which include probing the dynamics and folding of proteins (*11*−*16*) and nucleic acids (*9*, *17*, *18*), the function of molecular motors (*19*−*22*), the motions of proteins in membranes (*23*−*26*), and viral infection (*27*, *28*).

SINGLE-MOLECULE TECHNIQUES

In order to obtain useful information about biological systems through single-molecule methods, spectroscopic techniques are needed that are sensitive to molecular mechanisms or conformations. There are many techniques to choose from. For example, fluorescence polarization is sensitive to molecular orientational mobility (*29*−*31*); fluorescence intensity changes can probe enzyme function (*32*); and Förster resonance energy transfer (FRET) can detect changes in intramolecular or intermolecular distances (*12*, *15*, *33*−*36*). Therefore, the emergence of single-molecule spectroscopy over the past decade has added powerful new tools for studies of biochemical systems. This review will focus in particular on a subset of these methods as they have been applied in our laboratory to the dynamics and interactions of CaM.

Single-Molecule Techniques for Freely Diffusing Molecules. Detecting single molecules as they diffuse freely in solution (see Figure 2) circumvents the need for schemes to immobilize the molecules. This simplifies sample preparation and avoids the risk of perturbing the behavior of the probed molecules by restricting them at a surface or in a matrix. The excitation beam is simply focused into a small volume of sample containing fluorescence-labeled molecules. As fluorescence-labeled molecules diffuse through the focal region of the microscope, they emit fluorescence bursts, which are detected and analyzed in real time or recorded for later processing. Burst fluorescence methods go back to some of the earliest applications of single-molecule detection (*2*, *5*, *6*, *37*−*40*). Detection of multiple fluorescence parameters including photon arrival times, fluorescence lifetimes, fluorescence anisotropy, and emission wavelength provides additional information that can be used to identify and sort molecules (*41*−*43*). Burst methods allow high time resolution, so that molecular dynamics can be probed down to the microsecond time scale (*12*, *15*, *34*, *44*). The method is limited, however, by the time window of the average transit time of molecules through the focal region, typically ~1 ms. Thus tracking single-molecule properties for longer time periods requires a different approach involving restriction of translational diffusion of the molecule.

Burst measurements are closely related to fluorescence correlation spectroscopy (FCS), which was first developed in the 1970s (*45*, *46*). In FCS, as in burst measurements, molecules are detected as they diffuse through the focal region of the microscope. Fluctuations in fluorescence signals are analyzed by autocorrelation and cross correlation of signals from one or more fluorophores. Any dynamic process that modulates the fluorescence can contribute to the FCS signal. Thus, FCS is sensitive to translational diffusion, molecular interactions, kinetics, triplet dynamics, and intramolecular motions (*44*, *47*−*50*). Dynamics can be probed over a large time range, from nanoseconds to milliseconds, limited at short times by the photon count rate and at long times by the transit time of molecules through the focal region of the beam. Interpretation of FCS results is less direct than many other methods, involving calculation and analysis of correlation functions.

FRET in Single Molecules. With its sensitivity to intramolecular distances and dynamics FRET is powerful when applied at the single-molecule level. Single-molecule FRET was first demonstrated in DNA oligomers a decade ago (*33*) and has been applied in numerous studies since then (see refs *51*−*54* for reviews). In our lab, we set out to probe conformations of CaM at the single-molecule level by FRET.

In FRET, energy is transferred from an excited fluorophore (the "donor" D) to another fluorophore (the "acceptor" A) by dipole−dipole coupling over distances of tens of angstroms (*55*, *56*). The efficiency of energy transfer depends on distance to the sixth power and can be measured either from the relative fluorescence intensities of D (I_D) and A (I_A) fluorophores or from the fluorescence lifetimes of D in the absence (τ_D) or presence (τ_{DA}) of A. Detection of single-molecule FRET by D and A intensities requires two photon-counting detectors such as avalanche photodiodes (APDs) or a CCD detecting dual colors (*57*). While the lifetime method requires only a single detector, a pulsed laser is

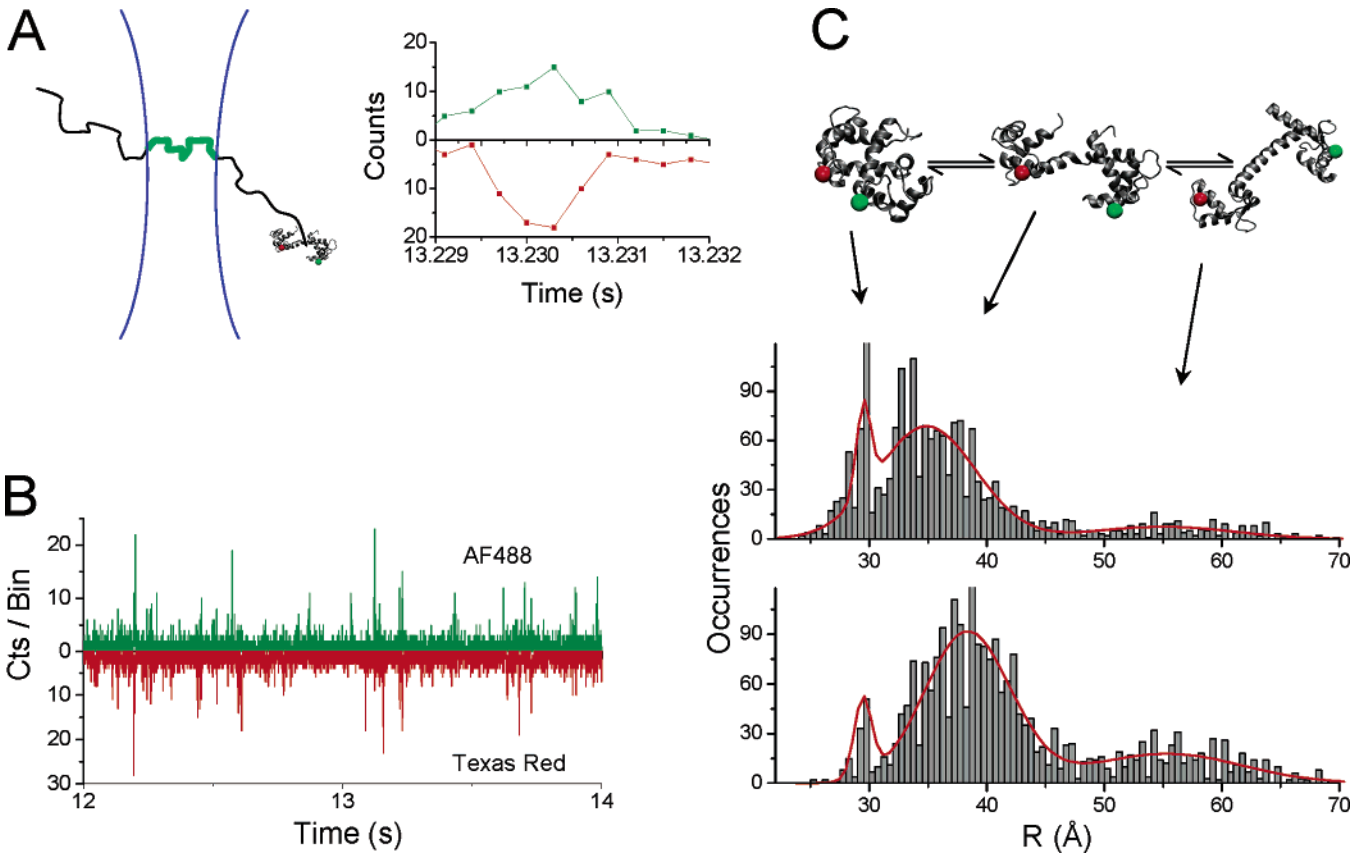

FIGURE 2: (A) Illustration of excitation of a freely diffusing CaM-DA molecule yielding a fluorescence burst as a CaM molecule diffuses through the focal region. The inset shows an expanded plot of a single burst of donor (Alexa Fluor 488) and acceptor (Texas Red) fluorescence counts collected in 300 μs time bins. (B) Single-molecule FRET data. The sample was excited at 488 nm. Bursts of high fluorescence correspond to single CaM-DA molecules traversing the focal region. The top panel shows emission from the donor fluorophore, and the bottom panel emission from the acceptor fluorophore. The CaM concentration was 100 pM. (C) CaM-DA distance distributions showing conformational substates of CaM measured by FRET between the donor fluorophore AlexaFluor 488 and the acceptor fluorophore Texas Red, attached to Cys residues mutated into CaM at sites 34 and 110. The FRET efficiency was calculated in 300 μs time bins from the measured D and A fluorescence counts, and the corresponding distances histogrammed as described in the text. Top: 25 μM Ca^{2+}. Bottom: 150 nm Ca^{2+}. Models at the top show possible structures of conformational substates of CaM: compact (left), bent (center), and extended (right).

needed for excitation and signals must be processed by time-correlated single photon counting.

With assumptions about the role of D and A orientational averaging (discussed below) the distance R between D and A is given by

$$\left(\frac{R}{R_0}\right)^6 = \frac{I_D}{\gamma(I_A - cI_D)} = \frac{\tau_{DA}}{\tau_D - \tau_{DA}} \quad (1)$$

where γ is a correction factor for the relative detection efficiencies of D and A fluorescence, cI_D corrects for cross-talk of D fluorescence in the A channel, and R_0, the Förster radius, is the distance at which the efficiency of energy transfer is 50%. For accurate intensity-based FRET measurements both intensities must be corrected for background counts. R_0 depends on a number of factors, including the quantum efficiency of D, the absorption coefficient of A, the overlap between the emission spectrum of D and the absorption spectrum of A, and, notoriously, the relative orientations of D and A (*56*). Usually these relative orientations are not precisely known and an orientationally averaged value is assumed, but this assumption must be checked. Given this assumption, the value of R_0 can be computed by numerical integration of the overlap of the fluorescence emission spectrum of D with the absorption spectrum of A (*56*). Typically for visible dye pairs, R_0 has a value between 45 and 60 Å.

Recently, several laboratories have used single-molecule detection to test the validity of common assumptions about FRET (*35*, *58*, *59*). In measurements with dyes attached to various lengths of polyproline, deviations from the energy transfer predicted by eq 1 were observed, implicating incomplete orientational averaging or breakdown of the point-dipole approximation (for short distances) and intramolecular dynamics (for longer distances) (*60*).

One of the most severe limitations in applying FRET to single-protein molecules is the need to attach two dye molecules to specific locations of the protein. Protein sites must be identified where D and A labels can be specifically attached, typically at Cys residues or amino groups or by fusion to fluorescent proteins. For some proteins, many such sites exist naturally, so that undesired competing sites must be eliminated by mutation. The possible effect of mutations and labeling on the biological activity of the protein must be checked. Once labeling sites are identified, for analysis of single-molecule signals it is necessary to sort DA-labeled molecules from other species present, e.g., molecules doubly labeled with either D or A, DD or AA, or singly labeled molecules (D or A). In some cases, this separation can be

achieved at the labeling step by exploiting different labeling chemistries or labeling rates for D and A labels. In other cases, DA-labeled molecules can be separated from other species after labeling, for example by HPLC (*61*). When neither of these methods is feasible, DA-labeled molecules can be sorted from other species at the signal level by checking for the presence of both D and A signals in single-molecule bursts. Photophysical phenomena such as triplet-state formation or other blinking effects can interfere with FRET measurements and therefore should be characterized for the dyes used (*58*). Photobleaching can also limit single-molecule FRET, and sorting methods can check for loss of D or A by photobleaching (*62*). Methods for such sorting include setting threshold signals levels in both D and A channels (*42*, *63*), examining the D lifetime in parallel with FRET efficiency (*14*), and alternately exciting D and A (*43*, *57*, *64*). The latter approach provides the clearest control for presence of D and A in single molecules, but with the added requirement for two collinear laser beams aligned through the microscope onto the sample.

Another challenge in single-molecule FRET experiments is to decode information about the molecular dynamics and conformations that is embedded in the stream of detected photon counts. Most current methods are coarse-grained, accumulating data into time bins. Although this approach is relatively simple, it is overly conservative, resulting in loss of information. New methods are needed to bring out the underlying information on kinetics, dynamics, and conformations. Work is starting to appear along these lines based on maximum likelihood estimators and statistical analysis (*65*−*70*). Other recent analytical approaches are aimed at improved precision of measurement in analysis of FRET efficiency distributions (*71*).

Single-Molecule Polarization Methods. The probability of absorption of light by a single molecule depends on the relative orientation of the molecular absorption transition dipole and the polarization of the excitation light. Similarly, the polarization of emitted fluorescence photons depends on the orientation of the emitting dipole. The response of a single molecule to polarized light and the polarization of emitted fluorescence therefore carry information about the orientation and orientational mobility of single molecules (*4*, *72*, *73*). Polarization methods have been applied to track the orientations of CaM bound to myosins, yielding detailed information about the mechanisms of motor-protein processivity (*19*, *30*, *74*). In these experiments, the polarization of the excitation beam was alternated approximately every 10 ms and the fluorescence polarization detected. The method requires modulation of the polarization of one or more excitation beams (for example with Pockels cells) and detection of fluorescence in multiple polarization channels.

Our implementation of single-molecule polarization modulation spectroscopy involves rotation of the excitation polarization (*31*, *75*−*77*). Although this approach yields less detailed information than multiple-channel measurements, it requires only one excitation channel and one detection channel to track orientational mobility. As the polarization of the excitation beam is rotated, the depth of modulation of single-molecule fluorescence measures the orientational mobility of the fluorescent molecule. The modulation depth is sensitive to orientational mobility in the plane of the rotating polarization. Orientation of the transition dipole out of this plane can also decrease the modulation depth due to a component of the electric field along the axial direction at the focus of a high numerical aperture objective, but the contribution is minor (*31*). Because the modulation depth depends on the ratio of modulation to average fluorescence intensity, it probes the orientational mobility of molecules in their ground electronic state and is not sensitive to fluctuations in fluorescence lifetime or fluorescence quantum yield. In this sense, it is akin to a linear dichroism measurement. The method can probe orientational mobility on time scales from hundreds of microseconds to milliseconds or longer. By varying the rate of polarization rotation by a Pockels cell, information about the time scale of orientational motion can also be generated.

CALMODULIN CONFORMATONS AND DYNAMICS

Biological signals are frequently transmitted by Ca^{2+} ions. A central link in Ca^{2+} signaling pathways is calmodulin (CaM), a Ca^{2+}-activated molecular switch (*78*, *79*). CaM is a small (16.7 kDa), acidic protein with two globular domains connected by a central linker (see Figure 1). Each domain contains two EF-hand sites that bind Ca^{2+} ions when the Ca^{2+} concentration rises above resting Ca^{2+} concentrations of around 100 nM (reviewed in ref *80*). Upon binding Ca^{2+}, the EF-hand domains open, exposing hydrophobic protein domains that can bind a wide range of target proteins (*1*, *81*, *82*). The response of CaM to Ca^{2+} and its interaction with target proteins therefore regulate many important cellular functions such as gene expression, neurotransmission, ion transport, smooth muscle contraction, neuronal plasticity, learning, and memory formation (*83*). How these responses occur and are relayed to target enzymes depends on the interplay of protein conformational changes and protein−protein interactions.

For Ca^{2+}-CaM, the first crystal structures showed an extended, dumbbell-shaped molecule with two globular domains linked by a central helix (*84*, *85*). Biochemical (*86*, *87*) and structural (*88*) studies, however, suggested a much more flexible structure of CaM in solution. In fact, an NMR structure did not resolve the relative orientations of the opposing N-terminal and C-terminal domains of Ca^{2+}-CaM (*88*), indicating considerable conformational flexibility. Remarkably, a recent crystal structure of Ca^{2+}-CaM showed a compact conformation of CaM (*89*) (also shown in Figure 1), further demonstrating that Ca^{2+}-CaM can exist in a range of possible conformations. However, each of these structural methods measures an ensemble-averaged structure that does not reveal the underlying distribution of conformations present, leaving unanswered the question of the actual distribution of conformations.

Conformational Substates of CaM. What conformations are actually present in solution? Are there identifiable conformational substates? In order to answer these questions, we used single-molecule FRET measurements with CaM freely diffusing in solution (*63*, *90*, *91*). Other experiments had previously detected a two-component fluorescence lifetime decay of a FRET donor (*92*). We attached fluorescent dyes to Cys residues introduced into the opposing globular domains of CaM (*61*, *93*) (see Figure 1). The FRET constructs labeled with D and A dyes are termed CaM-DA.

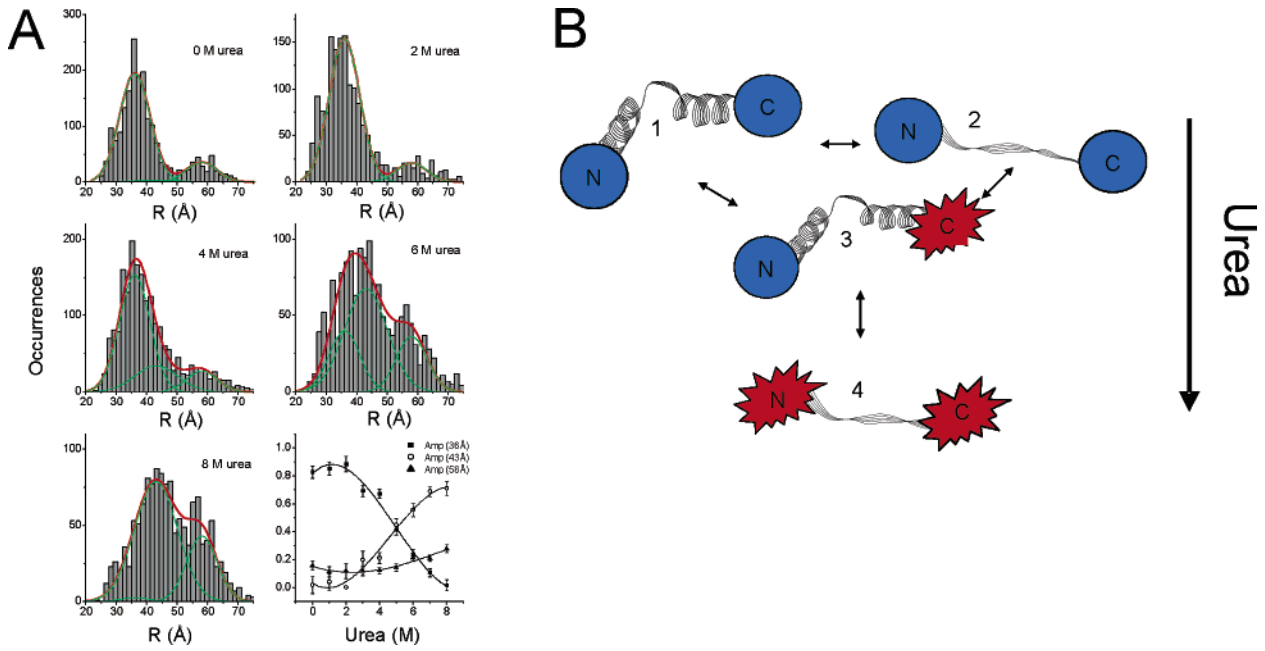

FIGURE 3: (A) Single-molecule CaM-DA distance distributions at varying urea concentrations (0.15 μM Ca^{2+}, 0.1 M KCl, 1 mM $MgCl_2$, pH 7.4). Distance histograms were determined as described in Figure 2. The solid lines show fits with three populations modeled as Gaussian functions where the centers and widths are fixed and only the amplitudes are varied. The lower right-hand plot shows the variations of these amplitudes with urea concentration. The population with center at 36 Å corresponds to the intermediate conformational substate detected under native conditions. The population centered at 43 Å is interpreted as an unfolding intermediate corresponding to denaturation of the C-terminal domain of apoCaM. The population centered at 58 Å comprises the extended conformation of CaM observed under native conditions and an extended denatured conformation that forms at high urea concentrations. Adapted from ref *99*. (B) Illustration of possible unfolding pathways for CaM (see similar scheme proposed in ref *98*). Structures 1 and 2 represent conformational substates present under native conditions. Structure 3 is an unfolding intermediate that forms at urea concentrations above 2 M as the population of 1 decreases. Extended conformations of denatured CaM (structure 4) are not significantly populated except at high urea concentrations (>4 M). Adapted from ref *99*.

For each single-molecule burst, fluorescence counts from D and A were binned (in time bins of 75 μs to 800 μs) and the ratio of fluorescence from D and A, corrected for cross-talk and the relative detection efficiencies of D and A channels (see eq 1), was used to calculate the distance between dyes. The distribution of distances R between D and A, shown in Figure 2, demonstrates that distinct conformational substates of CaM are indeed present in solution. The existence of these states had not previously been demonstrated.

The single-molecule FRET distributions reveal a wide range of conformational states of CaM. Conformations with D−A distances less than 30 Å demonstrate the existence of compact conformations while conformations with D−A distances of over 50 Å show that extended conformations are also present. The familiar dumbbell-like crystal structure of Ca^{2+}-CaM (see Figure 1) predicts a distance of around 55 Å between labeling sites (residues 34 and 110). This suggests that the extended conformational substate observed in the single-molecule FRET distributions may resemble this structure. In contrast, the conformational substates of CaM with the largest population do not correspond to any of the known crystal structures, but are consistent with reports that the central linker of Ca^{2+}-CaM is bent in solution (*94*). For apoCaM, a solution structure predicts a distance between labeling sites of 38 Å (1CFD (*95*)), and this is consistent with the intermediate conformational substate detected for apoCaM (Figure 2).

Thus the single-molecule FRET distributions demonstrated for the first time the presence of at least three discrete conformations of Ca^{2+}-CaM and apoCaM in solution. The population of conformational substates is Ca^{2+} dependent. The extended conformational state has a higher population for apoCaM, while the compact conformation has a higher amplitude for Ca^{2+}-CaM.

What might be the functional role of conformational substates of CaM? Several possibilities can be postulated. First, the conformations of CaM bound to targets span a wide range of geometries (*1*). The existence of a range of conformations, from compact to extended ones, may facilitate recognition and interaction of CaM with different target binding domains in diverse binding geometries. Second, the presence of a compact conformation for Ca^{2+}-CaM might provide a means for interdomain contacts. Several lines of evidence indicate communication between opposing domains of CaM (*96*, *97*), but the coupling mechanism has been unclear. The existence of a compact conformation provides a possible mechanism for the propagation of structural information from one domain to the other.

Unfolding Conformations of CaM. What happens to the conformational substates of CaM as it unfolds? The presence of distinct N- and C-terminal domains connected by a central linker raises the possibility that CaM may unfold in distinct steps. Studies showed that denaturation of the intact apo protein cannot be described simply as the sum of the unfolding of isolated N- and C-terminal domains (*96*, *98*).

The CaM-DA construct affords the opportunity for more detailed information about the unfolding pathway of CaM (*99*). FRET distributions for CaM are shown in Figure 3 as a function of urea concentration. Conformational substates are evident at each urea concentration. The distributions both broaden and shift to longer distances, and the population of an extended conformation increases as the urea concentration

increases. The shift and broadening of the distributions cannot be described simply as the disappearance of a native conformation and the appearance of an extended conformation. Therefore, in contrast to a two-state folding mechanism, the folding landscape of CaM possesses, at a minimum, at least one significantly populated intermediate structure between native and unfolded states, consistent with thermal stability measurements (*96*, *98*).

The simplest description describes the unfolding pathway in terms of a single unfolding intermediate. To test this model, we fit the distributions with three conformational substates having fixed centers and widths, allowing only their amplitudes to vary at different urea concentrations. These fits, shown in Figure 3, reveal several interesting features of CaM unfolding. First, the distributions can be described by an unfolding intermediate with a peak D−A distance of 43 Å. This is more elongated than the intermediate conformational substate detected under native conditions (D−A distance 36 Å for apoCaM) but shorter than the extended conformational substate (about 55 Å). The D−A distance of 43 Å indicates an intermediate unfolding conformation that is not fully extended, consistent with denaturation of one of the domains of CaM. The unfolding intermediate is present even at urea concentrations of 8 M urea, suggesting that native-like conformations of CaM continue to exist even at high urea concentrations. At urea concentrations above about 6 M, the population of an extended conformation with D−A distances of 55 to 65 Å begins to increase. This distance, which is similar to the D−A distance of the extended conformational substate of CaM under native conditions, is shorter than expected in a random-coil, suggesting that even this extended conformation retains native-like structural elements. This result is consistent with recent simulations that suggest that average end-to-end distances in denatured proteins may not differ substantially from end-to-end distances for proteins maintaining specific structural features (*100*−*102*).

CaM Conformational Dynamics. Given that CaM exists in conformational substates, an important question is how fast these states interchange. Conformational substates of CaM were observed in FRET distributions with bin times up to 800 μs (*63*, *90*). (Longer bin times are not possible due to the transit time of freely diffusing molecules through the focal region.) If conformational interchange occurred on a faster time scale, conformational averaging would result in narrowing of the FRET distribution. The absence of such narrowing shows that the conformational interchange must occur on a longer time scale.

In order to explore further the time scale of conformational interchange, single-molecule fluorescence-burst FRET trajectories were selected with durations of several milliseconds. Figure 4 shows a plot of several trajectories that track the conformational substate of CaM over periods of up to a few milliseconds. Occasional jumps from one conformational substate to another occur on the millisecond time scale. Interchange on this time scale has implications for the function of CaM. The millisecond interchange of conformational substates of CaM may permit rapid exploration of conformational space for molecular recognition of target binding domains. Interchange on this time scale further implies that experiments with longer effective probing times (e.g., NMR NOE measurements) yield an average over the properties of conformational substates having quite different interdomain conformations.

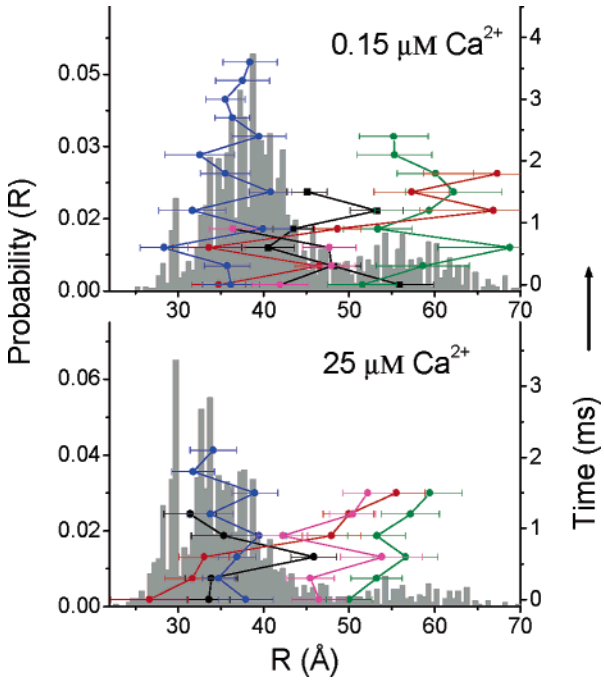

FIGURE 4: Single-molecule trajectories showing several examples of conformational interchange. The trajectories show D−A distances calculated from D and A fluorescence counts in sequential 300 μs bins in long-duration bursts. The single-molecule distributions at 0.15 μM Ca^{2+} (top) and 25 μM Ca^{2+} are shown in the background. Most trajectories remain in the same conformational substate, but occasional jumps are observed. Analysis shows that conformational exchange is not associated with changes in total intensity, and therefore is not likely related to the presence of more than one molecule (*91*). Adapted from ref *91*.

We also used FRET coupled with fluorescence correlation spectroscopy (FCS) to probe the dynamics of CaM in solution (*63*). Nanosecond orientational motions of CaM tethered to a surface were previously probed by single-molecule fluorescence anisotropy measurements (*103*). FCS coupled with FRET affords a sensitive probe of intramolecular fluctuations on the microsecond and millisecond time scales. This is the time scale on which functional motions of proteins often occur (*104*, *105*), but it has often been difficult to probe motions on this time scale. FCS−FRET can be used to probe these motions because, as the distance between D and A fluorophores fluctuates, the FRET efficiency also fluctuates, and these fluctuations can be detected, for example in the cross correlation between D and A fluorescence intensities. FRET fluctuations give rise to an anticorrelation between D and A intensities, resulting in a negative contribution to the cross-correlation function. Decay of the anticorrelation component contributes a rising component in the cross-correlation function on the time scale of dynamic fluctuations (*15*, *106*−*108*). FRET fluctuations also contribute a decay component to the autocorrelations of D and A intensities. Our approach involves global analysis of the complete set of second-order correlation functions: the autocorrelation in the D channel $G_{DD}(\tau)$, the autocorrelation in the A channel $G_{AA}(\tau)$, the cross correlation of D with A $G_{DA}(\tau)$, and the cross correlation of A with D $G_{AD}(\tau)$. The correlations shown in Figure 5 contain information about both the intramolecular and translational dynamics of the

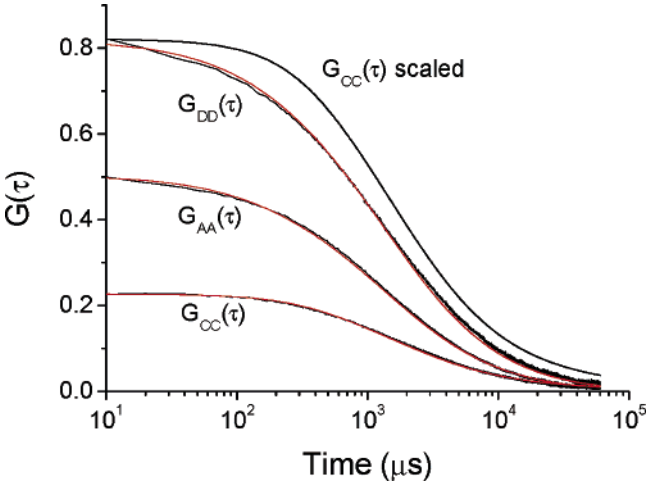

FIGURE 5: FCS and FCCS correlations for Ca^{2+}-CaM-DA with global fit. $G_{DD}(\tau)$ and $G_{AA}(\tau)$ are the autocorrelations of donor and acceptor. $G_{CC}(\tau)$ is the average of the cross correlations $G_{DA}(\tau)$ and $G_{AD}(\tau)$. The initial amplitudes differ because of different effective probe volumes. A $G_{CC}(\tau)$ curve scaled to the same initial value as $G_{DD}(\tau)$ is also plotted to illustrate their different time dependences due to intramolecular dynamics. The fit yields time constants of 140 μs and 1.4 ms for intramolecular dynamics, plus a longer-time component. The donor dye AlexaFluor 488 was excited by a laser beam generating fluorescence bursts from donor (directly excited by the laser) and acceptor (excited by FRET). The CaM-DA concentration was ~10 nM with count rates of 20 000 to 30 000 per second.

labeled molecules. The full correlation function incorporating fluctuations from diffusion and from intramolecular dynamics can be written (*15*)

$$G_{XY}(\tau) = a_{XY}[G^{d}_{XY}(\tau) \pm f_{XY}E(\tau)] \quad (+ \text{ for } X = Y, - \text{ for } X \neq Y) \quad (2)$$

where $G^{d}_{XY}(\tau)$ is the correlation function for translation diffusion, $E(\tau)$ describes the intramolecular dynamics, and a_{XX} and a_{XY} are scaling factors that allow for differences in the $\tau = 0$ values of the functions resulting from different probe volumes in the D and A channels. Results for Ca^{2+}-CaM and apoCaM showed that intramolecular fluctuations occur on the time scales of hundreds of microseconds and several milliseconds (*63*, *109*).

CALMODULIN−TARGET INTERACTIONS

CaM relays Ca^{2+} signals by binding to specific domains of target proteins. A CaM target database (*110*) currently contains some 300 sequences known to bind CaM. Deciphering the mechanisms of recognition and binding of a target is important for understanding the regulation of target proteins. Therefore a great deal of attention has been focused on the rates and equilibrium constants for CaM binding to peptides that represent the CaM-binding domains of target enzymes (see for example refs *92* and *111*−*113*). A number of structures are also now available of CaM−peptide complexes (reviewed in ref *1*).

It may be possible to answer a number of outstanding questions about CaM−peptide interactions by single-molecule methods. Are the conformations of these complexes static, or do they fluctuate among conformational substates? How do the N- and C-terminal domains of CaM interact with the peptide in the process of molecular recognition and

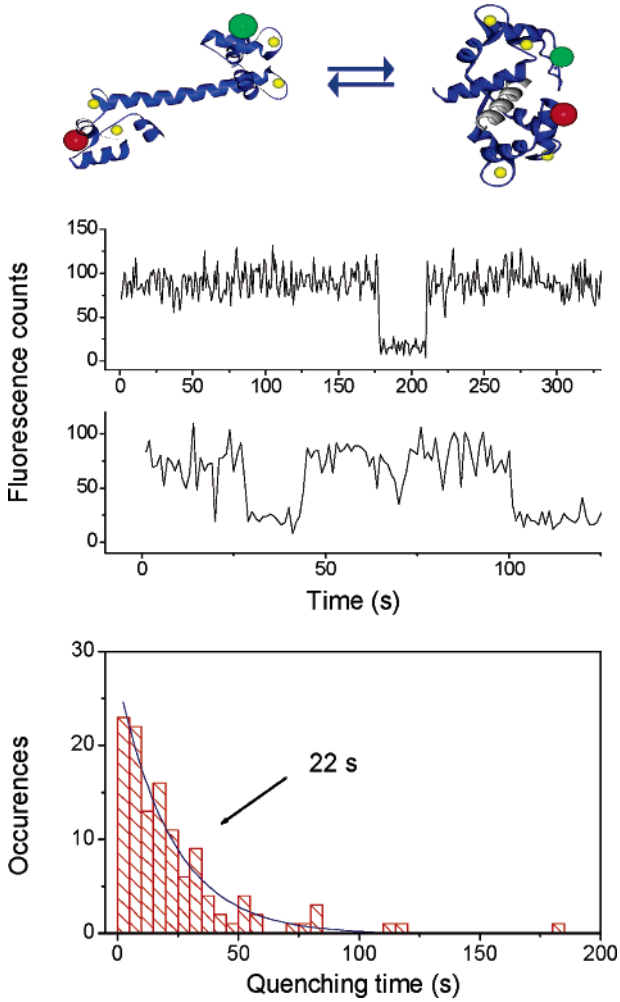

FIGURE 6: Fluorescence trajectories for C28W binding to MBP-CaM-AF488 immobilized in an agarose gel (2%), showing periods of fluorescence quenching. The MBP-CaM-AF488 concentration was 10 nM, and the C28W concentration was ca. 100 nM. The bottom panel shows a histogram of quenching persistence times yielding an off time of 22 s. Adapted from ref *118*.

binding? What are the intermediate states in CaM−peptide binding? The first detection of single-molecule CaM−target binding was demonstrated in the Moerner laboratory with a "cameleon" fusion protein consisting of CaM, ECFP and EYFP fluorescent proteins, and the CaM-binding domain of myosin light-chain kinase (*114*). Fluctuations were observed that were dependent on Ca^{2+} concentration. Hochstrasser and co-workers detected binding of a fluorescently labeled synthetic peptide to CaM encapsulated in a hydrogel with evidence for a heterogeneous binding-site environment, particularly at intermediate Ca^{2+} levels (*115*). Lu and co-workers have detected conformational states of CaM complexes with a 28-residue segment of the CaM binding domain of PMCA (*116*).

Results from our lab showed that single peptide binding events can be detected (see Figure 6). We detected binding of CaM to the peptide C28W, the CaM binding domain of PMCA, the plasma-membrane Ca^{2+} pump (*117*). Since peptide binding and release by CaM occurs on the time scale of seconds, it was necessary to immobilize CaM so that single-molecule signals could be recorded for periods of seconds to detect peptide binding. Our approach was to construct a fusion protein of CaM with a larger protein,

maltose binding protein, which serves as an anchor permitting immobilization of the fluorescently labeled fusion protein (MBP-CaM-AF488) in a low weight-percent (1−2%) agarose gel (*61*). Because binding of C28W results in quenching of MBP-CaM-AF488 fluorescence by a tryptophan residue in the peptide, fluorescence quenching can be used to track peptide binding (*118*). Single-molecule trajectories in Figure 6 illustrate MBP-CaM-AF488 quenching by binding C28W. A histogram of the persistence times for quenching yields a peptide off time of 22 s. This result illustrates the possibility of measuring binding and release kinetics for small quantities of protein at equilibrium, without the kinetic synchronization needed for ensemble measurements as in stop-flow kinetics, for example.

Peptide binding can also be detected by the change in distance between D and A in CaM-DA. As above, fusion of CaM with MBP permits immobilization of MBP-CaM-DA in an agarose gel. We used MBP-CaM-DA to detect CaM binding with the CaM binding domain of CaM-dependent protein kinase II (CaMKII). With the FRET pair available for these studies, peptide binding brings the fluorophores attached to Cys residues 34 and 110 into close proximity so that fluorescence from both dyes is quenched as a result of close dye−dye interactions (*93*). This peptide contains no Trp residue, so peptide binding does not significantly alter the fluorescence of singly labeled CaM (e.g., CaM-AF488). However, it is possible to use the fluorescence from the CaM-DA dye pair as an on or off signal for peptide binding at the single-molecule level. We titrated the binding of the CaMKII peptide to MBP-CaM-DA by counting single-molecule signals in a 20 × 20 μm^2 scan at a low CaM concentration, yielding a dissociation constant of 103 ± 35 pM (*93*). Information about the conformations of CaM bound to the peptide is not available with the 34-110 CaM dye-pair construct because of the close dye interactions. In future work, we plan to use other fluorescence labeling sites where D and A are more separated.

REGULATION OF PLASMA-MEMBRANE CALCIUM ATPASE

Because CaM is involved in many essential cellular functions, determining the mechanisms of interaction of CaM with the proteins that it regulates will help our understanding of cellular signaling pathways. Many CaM-activated enzymes are regulated by an autoinhibitory domain, which blocks access or function at the catalytic site (*1*). In our laboratory, we have studied the activation of PMCA, a Ca^{2+} pump that functions to maintain the low intracellular Ca^{2+} levels necessary for Ca^{2+} signaling (*119*, *120*). A better understanding of PMCA regulation will further our understanding of the mechanisms that maintain Ca^{2+} homeostasis in cells.

PMCA is a 134 kDa protein with ten transmembrane segments (see Figure 7). A large intracellular loop between transmembrane segments 4 and 5 contains the ATP binding site and a phosphorylatable aspartate residue (*121*). The CaM binding domain is located in the autoinhibitory domain near the C terminus of PMCA (*117*). CaM binding triggers a conformational change that removes autoinhibition. The goal of experiments on PMCA in our laboratory is to understand the coupling between CaM binding, autoinhibitory domain conformation, and enzymatic cycling. Single-molecule methods are valuable in this system for uncovering substates and distributions of conformations. In addition, single-molecule spectroscopy is a useful approach to study proteins such as PMCA that are available in low abundance.

FIGURE 7: Predicted PMCA structure (130), with the extensive cytosolic portions of the enzyme toward the bottom. The structure was generated by homology and comparative modeling based on reported structures of the SERCA Ca^{2+} pump (*129*) with protein−protein docking and guidance from biochemical studies. The green and red regions show segments 206−271 and 537−554 (respectively) where the autoinhibitory domain is known to bind. The purple segment is the CaM binding domain. The phosphorylation site is shown in orange, and a lysine residue located in the ATP binding region is shown in blue. Figure courtesy of G. H. Lushington.

Polarization Modulation Spectroscopy. In our experiments on PMCA, we used single-molecule polarization modulation, illustrated in Figure 8. We developed a maximum likelihood estimator method to analyze fluorescence polarization modulation signals (*31*) in the low-count, Poisson-statistics limit of single-molecule spectroscopy. This analysis yields the modulation depth and phase as a function of time throughout the fluorescence trajectory, and the modulation depth can be used to track the orientational mobility of the fluorophore.

In order to apply single-molecule polarization methods to CaM, we constructed T34C-CaM and labeled the Cys residue with tetramethylrhodamine (TMR). PMCA purified from CaM-depleted erythrocyte ghost membranes was immobilized in agarose gels (∼2% by weight). CaM itself diffuses freely through such gels, but becomes translationally restricted when bound to the much larger PMCA (*31*, *76*). Single CaM-TMR molecules were not detected in the absence of either PMCA or Ca^{2+}, and thus molecules detected under these conditions can be identified as CaM-TMR bound to PMCA in a Ca^{2+}-dependent manner. Single PMCA−CaM-TMR complexes were located by scanning a piezoelectric scanner and excited by a 543 nm beam with polarization modulated at 25 Hz. We found that the translational mobility of PMCA−CaM-TMR complexes was restricted in agarose gels for periods of tens of minutes. The modulation depth was determined for each modulation period and averaged to give modulation depth for each molecule.

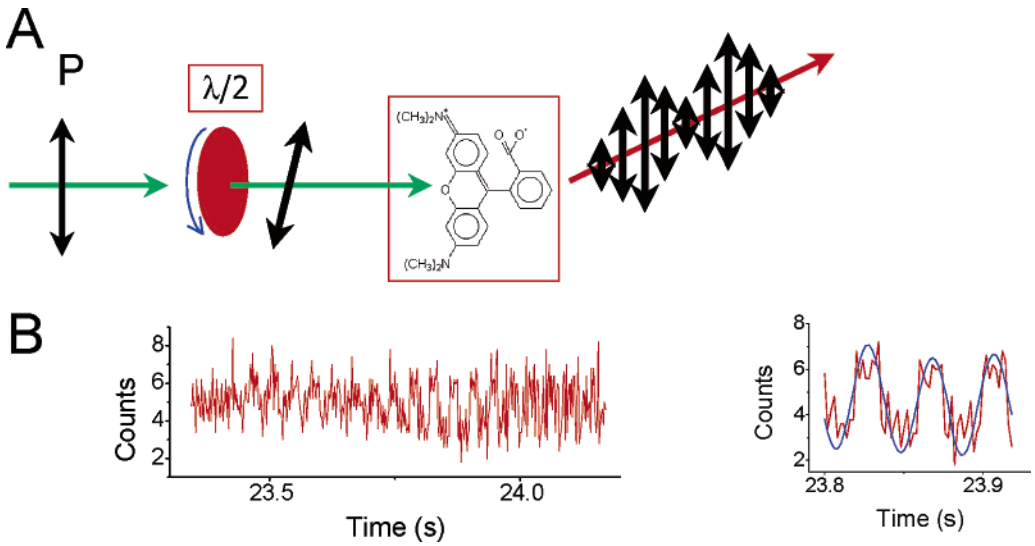

FIGURE 8: (A) Illustration of polarization modulation experiment. A laser beam coming from the left with linear polarization is passed through an electro-optic modulator and quarter waveplate combination, which function together as a half-wave ($\lambda/2$) retarder to rotate the polarization of the excitation beam. An orientationally immobile molecule has a high modulation depth because its excitation is modulated as the polarization rotates with respect to the dye's transition dipole. An orientationally mobile molecule on the other hand does not show modulated fluorescence because the molecule rapidly samples all orientations relative to the excitation polarization. (B) An example of a single-molecule polarization modulated trajectory (left) and maximum likelihood estimator fit (right).

Using the polarization modulation method, we measured the modulation depths of CaM-TMR bound to PMCA under saturating and subsaturating Ca^{2+} concentrations in the presence or absence of ATP (see Figure 9). At a saturating Ca^{2+} concentration, we found a single orientational-mobility population of molecules with a low modulation depth, consistent with CaM bound to a dissociated and mobile autoinhibitory domain (*76*). In contrast, at a lower Ca^{2+} concentration in the absence of ATP, a second population appears with a higher modulation depth, corresponding to a lower orientational mobility. The distribution of orientational mobilities shown in Figure 9 is not consistent with a two-state model of the activation of PMCA. In a two-state model, the autoinhibitory domain is associated with the nucleotide binding region of the pump in the absence of CaM and dissociated from the nucleotide binding region when CaM is bound. In this model, at a reduced Ca^{2+} concentration, fewer CaM molecules would be bound to PMCA because of the reduced affinity of CaM for PMCA binding at reduced Ca^{2+}, but those molecules that are bound to PMCA would have the same orientational mobility as at a higher Ca^{2+} concentration. Thus the presence of a lower mobility population a subsaturating Ca^{2+} demonstrates the existence of another state of CaM−PMCA complexes.

We proposed a model (illustrated in Figure 9) with an intermediate state in the activation of the pump in which CaM is bound but the autoinhibitory domain is still associated with the active site (*76*). In this model the orientationally more mobile population corresponds to PMCA−CaM complexes with a dissociated autoinhibitory domain of the Ca^{2+} pump and the less mobile population corresponds to PMCA with a nondissociated autoinhibitory domain (see Figure 9). This model is consistent with kinetic measurements that indicated that CaM can bind to PMCA in both its open (dissociated autoinhibitory domain) and closed (nondissociated autoinhibitory domain) forms (*122*). In our interpretation, the depth of polarization modulation provides a means to track the conformation of the autoinhibitory domain.

The Ca^{2+} and ATP dependences of these populations support their interpretation in terms of active and inactive PMCA (Figure 9). We found that in the presence of ATP, which is required for enzymatic cycling, only the high-mobility population is present, even at a reduced Ca^{2+} concentration. This indicates that when ATP is present, so that PMCA is actively cycling, the likelihood for the autoinhibitory domain to associate with the catalytic site is very small. This finding is supported by measurements of the susceptibility of PMCA to chymotrypsin proteolysis (*77*). Thus, enzymatic cycling alters the interaction of the autoinhibitory domain with the catalytic domain at subsaturating Ca^{2+}. The change in binding propensity of the autoinhibitory domain in the presence of ATP may occur as a result of an enzymatic conformational change associated with ATP hydrolysis and associated phosphorylation of the enzyme, as has been proposed for the homologous SERCA Ca^{2+} pump (*123*, *124*).

We have carried out further polarization-modulation experiments to probe the effect of oxidative modification on the distribution of orientational mobilities of PMCA−CaM complexes (*75*). Oxidative modification of either PMCA (*125*) or CaM (*126*) results in reduced PMCA activity. Single-molecule polarization modulation experiments yield insight into the mechanistic source of this activity loss. As shown in Figure 9, oxidation of CaM produces a significantly higher population of PMCA−CaM complexes with low orientational mobility (high modulation depth), suggesting that oxidative modification of CaM results in a reduced effectiveness of CaM to induce dissociation of the autoinhibitory domain (*75*). Even in the presence of ATP, which for nonoxidized CaM results in complete dissociation of the autoinhibitory domain, a substantial fraction of CaMox−PMCA complexes remains with a nondissociated autoinhibitory domain (Figure 9).

Similar experiments probed the effect of oxidative modification of PMCA on the mechanism of activation of PMCA (*77*). Again, a low-mobility (high modulation depth) distribu-

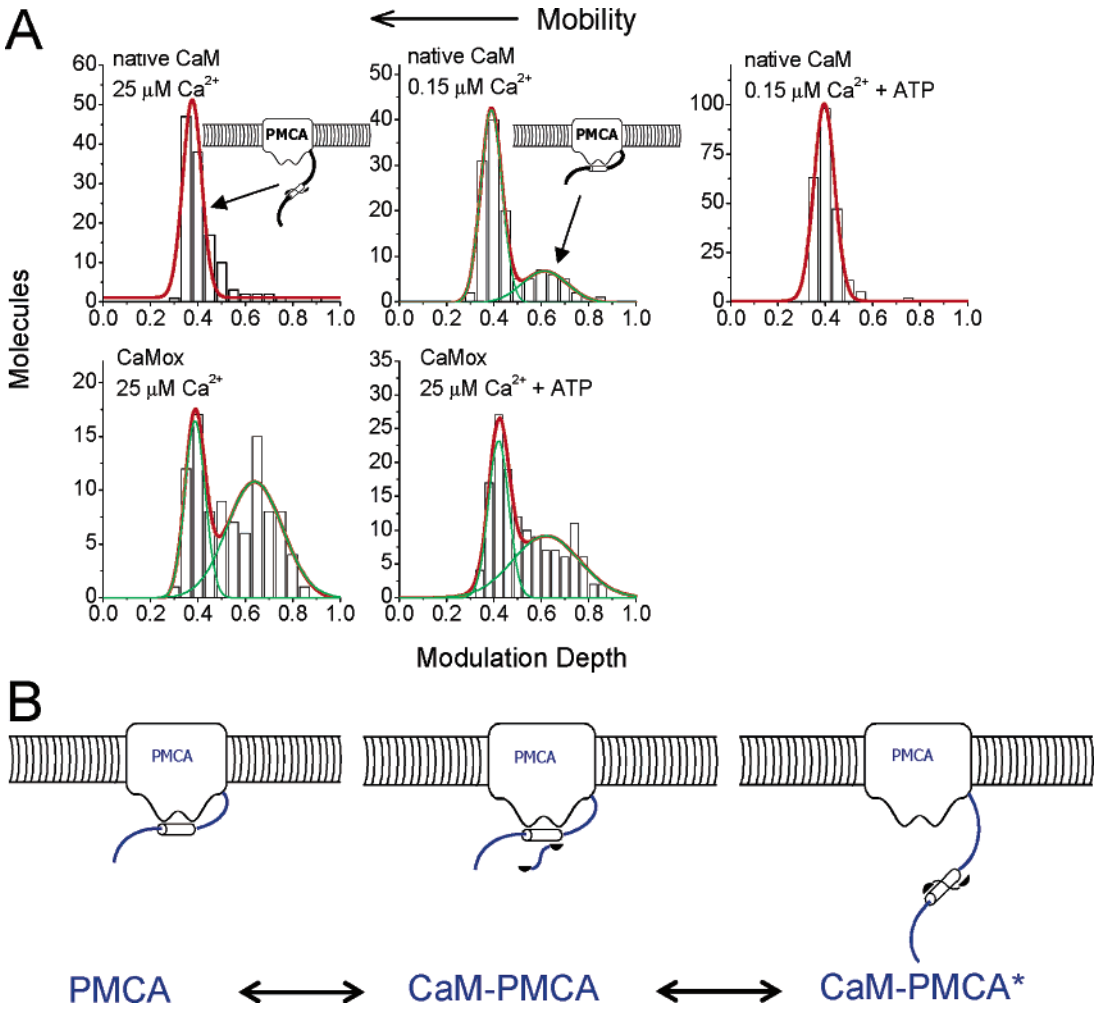

FIGURE 9: (A) Modulation depth histograms for complexes of PMCA with native CaM (top row) and CaMox (bottom row). A higher modulation depth corresponds to a lower orientational mobility. PMCA was immobilized in agarose gel, in which CaM-TMR diffuses. The histograms show the modulation depth for single PMCA−CaM-TMR complexes averaged over trajectories of several seconds duration (limited by photobleaching). At a high Ca^{2+} concentration CaM−PMCA complexes are nearly all in a high mobility state, which we attribute to CaM bound to a dissociated autoinhibitory domain (upper left panel). At a reduced Ca^{2+} concentration, a second, lower-mobility population appears, which we attribute to CaM bound to a nondissociated autoinhibitory domain (upper center panel). With the addition of ATP, the high-mobility population is recovered (upper right panel), indicating a conformational change that leads to a dissociated autoinhibitory domain even at a low Ca^{2+} concentration (upper right panel). The lower row shows the effect of oxidative modification of CaM. A large low-mobility population is present even at high Ca^{2+} (lower left panel) and in the presence of ATP (lower right panel), indicating a reduced potency of CaM to induce dissociation of the autoinhibitory domain. The solid lines show fits of the histograms to Gaussian functions with centers at modulation depths of around 0.40 (high-mobility population) or 0.62 (low-mobility population). Adapted from refs *75* and *76*. (B) Model for CaM activation of PMCA. Left: PMCA with nondissociated autoinhibitory domain. Center: PMCA−CaM complex with autoinhibitory domain not dissociated. Right: PMCA−CaM complex with autoinhibitory domain dissociated. The relative populations of PMCA−CaM complexes with dissociated and nondissociated autoinhibitory domains depend on Ca^{2+} concentration, ATP, and oxidative modification of CaM or PMCA.

tion remained in the presence of ATP for oxidized PMCA. In contrast, in the absence of ATP, the orientational mobility distributions closely resembled those for nonoxidized PMCA. In fact, the addition of ATP to PMCAox−CaM-TMR complexes resulted in a larger fraction of complexes with a low mobility. This result shows that coupling between the autoinhibitory domain and the nucleotide binding domain is altered by oxidative modification of PMCA in a way that leads to an increased population of complexes with a nondissociated autoinhibitory domain. It appears that PMCAox fails to undergo the conformational changes that occur in native PMCA that promote dissociation of the autoinhibitory domain after binding of ATP. These results show that the loss of activity resulting from oxidative damage is correlated with an altered interaction between the catalytic and autoinhibitory domains, even with CaM bound.

CONCLUSIONS AND FUTURE PROSPECTS

Over the past 10 years, single-molecule spectroscopy has progressed from an exotic technique practiced by specialists to a tool with real utility in the study of biological systems. This review shows that relatively straightforward implementation (a single excitation beam and one or two detection channels) of single-molecule methods such as burst-detected FRET or polarization modulation can yield new knowledge about conformational state distributions and dynamics. Conformational substates and intermediate states were revealed by these methods that had not previously been detected, both for CaM and for PMCA−CaM complexes. For CaM in solution, single-molecule measurements demonstrated the presence of conformational substates spanning a wide range of global conformations, from compact to

extended. The conformational interchange time appears to be on the millisecond time scale. For CaM bound to a target enzyme, PMCA, single-molecule distributions revealed a previously undetected intermediate state. We interpreted this state as a PMCA−CaM complex with a nondissociated autoinhibitory domain. The ability to detect conformational distributions of PMCA−CaM complexes led to information about how oxidative modification of either CaM or PMCA results in loss of activity through decreased effectiveness in dissociation of the autoinhibitory domain, resulting in an increased population of enzyme in the intermediate state. This illustrates the relevance of single-molecule measurements of the properties of distributions for understanding biological function.

As improvements are made in spectroscopic techniques, targeted labeling methods, detection sensitivity, and the development of fluorescent probes with greater brightness and stability, we expect that single-molecule fluorescent methods will be applied to more complex biological systems. Perhaps the most exciting challenge is the application of single-molecule spectroscopy to study processes in living cells. Application of these methods would provide a new tool for scientists investigating the network of CaM signaling processes in functioning cells. One of the factors limiting such experiments at present is the need for methods of introducing bright but biologically inert fluorescent probes as labels inside cells. The availability of methods to probe the interactions, dynamics, and conformations of single molecules as they function within the complex network of cellular processes promises to open a new and exciting chapter in answering important biological questions.

ACKNOWLEDGMENT

I am grateful to current and former students and postdoctoral associates who contributed much of the work reviewed in this paper: Michael W. Allen, Mangala Roshan Liyanage, Abhijit Mandal, Kenneth D. Osborn, E. Shane Price, Brian D. Slaughter, and Jay R. Unruh. I acknowledge insightful discussions with Greg Harms, Don Lamb, Claus Seidel, Tom Squier, Jeff Urbauer, and Asma Zaidi. I thank Ramona Bieber Urbauer for preparation of CaM mutants and the MBP-CaM fusion, and Asma Zaidi for preparation of PMCA.

REFERENCES

1. Hoeflich, K. P., and Ikura, M. (2002) Calmodulin in Action: Diversity in Target Recognition and Activation Mechanisms, *Cell 108*, 739−742.
2. Shera, E. B., Seitzinger, N. K., Davis, L. M., Keller, R. A., and Soper, S. A. (1990) Detection of Single Fluorescent Molecules, *Chem. Phys. Lett. 174*, 553−557.
3. Ambrose, W. P., and Moerner, W. E. (1991) Fluorescence Spectroscopy and Spectral Diffusion of Single Impurity Molecules in a Crystal, *Nature 349*, 225−227.
4. Xie, X. S., and Dunn, R. C. (1994) Probing Single Molecule Dynamics, *Science 265*, 361−364.
5. Nie, S., Chiu, D. T., and Zare, R. N. (1994) Probing Individual Molecules in Solution with Confocal Fluorescence Microscopy, *Science 266*, 1018−1021.
6. Eigen, M., and Rigler, R. (1994) Sorting Single Molecules: Application to Diagnostics and Evolutionary Biotechnology, *Proc. Natl. Acad. Sci. U.S.A. 91*, 5740−5747.
7. Moerner, W. E. (2002) A Dozen Years of Single-Molecule Spectroscopy in Physics, Chemistry, and Biophysics, *J. Phys. Chem. B 106*, 910−927.
8. Michalet, X., Kapanidis, A. N., Laurence, T., Pinaud, F., Doose, S., Pflughoefft, M., and Weiss, S. (2003) The Power and Prospects of Fluorescence Microscopies and Spectroscopies, *Annu. Rev. Biophys. Biomol. Struct. 32*, 161−182.
9. Ha, T. (2004) Structural Dynamics and Processing of Nucleic Acids Revealed by Single-Molecule Spectroscopy, *Biochemistry 43*, 4055−4063.
10. Min, W., English, B. P., Luo, G., Cherayil, B. J., Kou, S. C., and Xie, X. S. (2005) Fluctuating Enzymes: Lessons from Single-Molecule Studies, *Acc. Chem. Res. 38*, 923−931.
11. Schuler, B., Lipman, E. A., and Eaton, W. A. (2002) Probing the Free-Energy Surface for Protein Folding with Single-Molecule Fluorescence Spectroscopy, *Nature 419*, 743−747.
12. Talaga, D. S., Lau, W. L., Roder, H., Tang, J., Jia, Y., DeGrado, W. F., and Hochstrasser, R. M. (2000) Dynamics and Folding of Single Two-Stranded Coiled-Coil Peptides Studied by Fluorescent Energy Transfer Confocal Microscopy, *Proc. Natl. Acad. Sci. U.S.A. 97*, 13021−13026.
13. Deniz, A. A., Laurence, T. A., Beligere, G. S., Dahan, M., Martin, A. B., Chemla, D. S., Dawson, P. E., Schultz, P. G., and Weiss, S. (2000) Single-Molecule Protein Folding: Diffusion Fluorescence Resonance Energy Transfer Studies of the Denaturation of Chymotrypsin Inhibitor 2, *Proc. Natl. Acad. Sci. U.S.A. 97*, 5179−5184.
14. Rothwell, P. J., Berger, S., Kensch, O., Felekyan, S., Antonik, M., Wohrl, B. M., Restle, T., Goody, R. S., and Seidel, C. A. M. (2003) Multiparameter Single-Molecule Fluorescence Spectroscopy Reveals Heterogeneity of HIV-1 Reverse Transcriptase: Primer/Template Complexes, *Proc. Natl. Acad. Sci. U.S.A. 100*, 1655−1660.
15. Margittai, M., Widengren, J., Schweinberger, E., Schroeder, G. F., Felekyan, S., Haustein, E., Koenig, M., Fasshauer, D., Grubmueller, H., Jahn, R., and Seidel, C. A. M. (2003) Single-Molecule Fluorescence Resonance Energy Transfer Reveals a Dynamic Equilibrium between Closed and Open Conformations of Syntaxin 1, *Proc. Natl. Acad. Sci. U.S.A. 100*, 15516−15521.
16. Rhoades, E., Cohen, M., Schuler, B., and Haran, G. (2004) Two-State Folding Observed in Individual Protein Molecules, *J. Am. Chem. Soc. 126*, 14686−14687.
17. Rueda, D., Bokinsky, G., Rhodes, M. M., Rust, M. J., Zhuang, X., and Walter, N. G. (2004) Single-Molecule Enzymology of RNA: Essential Functional Groups Impact Catalysis from a Distance, *Proc. Natl. Acad. Sci. U.S.A. 101*, 10066−10071.
18. Kim, H. D., Nienhaus, G. U., Ha, T., Orr, J. W., Williamson, J. R., and Chu, S. (2002) Mg^{2+}-Dependent Conformational Change of RNA Studied by Fluorescence Correlation and FRET on Immobilized Single Molecules, *Proc. Natl. Acad. Sci. U.S.A. 99*, 4284−4289.
19. Rosenberg, S. A., Quinlan, M. E., Forkey, J. N., and Goldman, Y. E. (2005) Rotational Motions of Macro-Molecules by Single-Molecule Fluorescence Microscopy, *Acc. Chem. Res. 38*, 583−593.
20. Peterman, E. J. G., Sosa, H., and Moerner, W. E. (2004) Single-Molecule Fluorescence Spectroscopy and Microscopy of Biomolecular Motors, *Annu. Rev. Phys. Chem. 55*, 79−96.
21. Adachi, K., Noji, H., and Kinosita, K., Jr. (2003) Single-Molecule Imaging of Rotation of F1-ATPase, *Methods Enzymol. 361*, 211−227.
22. Yildiz, A., and Selvin, P. R. (2005) Fluorescence Imaging with One Nanometer Accuracy: Application to Molecular Motors, *Acc. Chem. Res. 38*, 574−582.
23. Schmidt, T., Schuetz, G. J., Baumgartner, W., Gruber, H. J., and Schindler, H. (1996) Imaging of Single Molecule Diffusion, *Proc. Natl. Acad. Sci. U.S.A. 93*, 2926−2929.
24. Harms, G. S., Cognet, L., Lommerse, P. H. M., Blab, G. A., Kahr, H., Gamsjager, R., Spaink, H. P., Soldatov, N. M., Romanin, C., and Schmidt, T. (2001) Single-Molecule Imaging of L-Type Ca^{2+} Channels in Live Cells, *Biophys. J. 81*, 2639−2646.
25. Lommerse, P. H. M., Blab, G. A., Cognet, L., Harms, G. S., Snaar-jagalska, B. E., Spaink, H. P., and Schmidt, T. (2004) Single-Molecule Imaging of the H-Ras Membrane-Anchor Reveals Domains in the Cytoplasmic Leaflet of the Cell Membrane, *Biophys. J. 86*, 609−616.
26. Deich, J., Judd, E. M., McAdams, H. H., and Moerner, W. E. (2004) Visualization of the Movement of Single Histidine Kinase Molecules in Live Caulobacter Cells, *Proc. Natl. Acad. Sci. U.S.A. 101*, 15921−15926.
27. Seisenberger, G., Ried, M. U., Endress, T., Buning, H., Hallek, M., and Brauchle, C. (2001) Real-Time Single-Molecule Imaging

of the Infection Pathway of an Adeno-Associated Virus, *Science 294*, 1929−1932.
28. Rust, M. J., Lakadamyali, M., Zhang, F., and Zhuang, X. (2004) Assembly of Endocytic Machinery around Individual Influenza Viruses During Viral Entry, *Nat. Struct. Mol. Biol. 11*, 567−573.
29. Ha, T., Enderle, T., Chemla, D. S., Selvin, P. R., and Weiss, S. (1996) Single Molecule Dynamics Studied by Polarization Modulation, *Phys. Rev. Lett. 77*, 3979−3982.
30. Forkey, J. N., Quinlan, M. E., Shaw, M. A., Corrie, J. E., and Goldman, Y. E. (2003) Three-Dimensional Structural Dynamics of Myosin V by Single-Molecule Fluorescence Polarization, *Nature 422*, 399−404.
31. Osborn, K. D., Singh, M. K., Urbauer, R. J. B., and Johnson, C. K. (2003) Maximum Likelihood Approach to Single-Molecule Polarization Modulation Analysis, *ChemPhysChem 4*, 1005−1011.
32. Lu, H. P., Xun, L., and Xie, X. S. (1998) Single-Molecule Enzymatic Dynamics, *Science 282*, 1877−1882.
33. Ha, T., Enderle, T., Ogletree, D. F., Chemla, D. S., Selvin, P. R., and Weiss, S. (1996) Probing the Interaction between Two Single Molecules: Fluorescence Resonance Energy Transfer between a Single Donor and a Single Acceptor, *Proc. Natl. Acad. Sci. U.S.A. 93*, 6264−6268.
34. Deniz, A. A., Dahan, M., Grunwell, J. R., Ha, T., Faulhaber, A. E., Chemla, D. S., Weiss, S., and Schultz, P. G. (1999) Single-Pair Fluorescence Resonance Energy Transfer on Freely Diffusing Molecules: Observation of Förster Distance Dependence and Subpopulations, *Proc. Natl. Acad. Sci. U.S.A. 96*, 3670−3675.
35. Schuler, B., Lipman, E. A., Steinbach, P. J., Kumke, M., and Eaton, W. A. (2005) Polyproline and The "Spectroscopic Ruler" Revisited with Single-Molecule Fluorescence, *Proc. Natl. Acad. Sci. U.S.A. 102*, 2754−2759.
36. Kapanidis, A. N., Laurence, T. A., Lee, N. K., Margeat, E., Kong, X., and Weiss, S. (2005) Alternating-Laser Excitation of Single Molecules, *Acc. Chem. Res. 38*, 523−533.
37. Nguyen, D. C., Keller, R. A., Jett, J. H., and Martin, J. C. (1987) Detection of Single Molecules of Phycoerythrin in Hydrodynamically Focused Flows by Laser-Induced Fluorescence, *Anal. Chem. 59*, 2158−2161.
38. Peck, K., Stryer, L., Glazer, A. N., and Mathies, R. A. (1989) Single-Molecule Fluorescence Detection: Autocorrelation Criterion and Experimental Realization with Phycoerythrin, *Proc. Natl. Acad. Sci. U.S.A. 86*, 4087−4091.
39. Whitten, W. B., Ramsey, J. M., Arnold, S., and Bronk, B. V. (1991) Single-Molecule Detection Limits in Levitated Microdroplets, *Anal. Chem. 63*, 1027−1031.
40. Soper, S. A., Davis, L. M., and Shera, E. B. (1992) Detection and Identification of Single Molecules in Solution, *J. Opt. Soc. Am. B 9*, 1761−1769.
41. Zander, C., Sauer, M., Drexhage, K. H., Ko, D.-S., Schulz, A., Wolfrum, J., Brand, L., Eggeling, C., and Seidel, C. A. M. (1996) Detection and Characterization of Single Molecules in Aqueous Solution, *Appl. Phys. B 63*, 517−523.
42. Eggeling, C., Berger, S., Brand, L., Fries, J. R., Schaffer, J., Volkmer, A., and Seidel, C. A. M. (2001) Data Registration and Selective Analysis for Single-Molecule Fluorescence Spectroscopy Using Bifl, *J. Biotechnol. 86*, 163−180.
43. Kapanidis, A. N., Lee, N. K., Laurence, T. A., Doose, S., Margeat, E., and Weiss, S. (2004) Fluorescence-Aided Molecule Sorting: Analysis of Structure and Interactions by Alternating-Laser Excitation of Single Molecules, *Proc. Natl. Acad. Sci. U.S.A. 101*, 8936−8941.
44. Edman, L., Mets, Ü., and Rigler, R. (1996) Conformational Transitions Monitored for Single Molecules in Solution, *Proc. Natl. Acad. Sci. U.S.A. 93*, 6710−6715.
45. Magde, D., Elson, E., and Webb, W. W. (1972) Thermodynamic Fluctuations in a Reacting System−Measurement by Fluorescence Correlation Spectroscopy, *Phys. Rev. Lett. 29*, 705−708.
46. Elson, E. L., and Magde, D. (1974) Fluorescence Correlation Spectroscopy. I. Conceptual Basis and Theory, *Biopolymers 13*, 1−27.
47. Chen, Y., Müller, J. D., Berland, K. M., and Gratton, E. (1999) Fluorescence Fluctuation Spectroscopy, *Methods 19*, 234−252.
48. Hess, S. T., Huang, S., Heikal, A. A., and Webb, W. W. (2002) Biological and Chemical Applications of Fluorescence Correlation Spectroscopy: A Review, *Biochemistry 41*, 697−705.
49. Chattopadhyay, K., Saffarian, S., Elson, E. L., and Frieden, C. (2002) Measurement of Microsecond Dynamic Motion in the Intestinal Fatty Acid Binding Protein by Using Fluorescence Correlation Spectroscopy, *Proc. Natl. Acad. Sci. U.S.A. 99*, 14171−14176.
50. Haustein, E., and Schwille, P. (2003) Ultrasensitive Investigations of Biological Systems by Fluorescence Correlation Spectroscopy, *Methods 29*, 153−166.
51. Kapanidis, A. N., Laurence, T. A., Lee, N. K., Margeat, E., Kong, X., and Weiss, S. (2005) Alternating-Laser Excitation of Single Molecules, *Acc. Chem. Res. 38*, 523−533.
52. Haas, E. (2005) The Study of Protein Folding and Dynamics by Determination of Intramolecular Distance Distributions and Their Fluctuations Using Ensemble and Single-Molecule FRET Measurements, *ChemPhysChem 6*, 858−870.
53. Ha, T. (2001) Single-Molecule Fluorescence Resonance Energy Transfer, *Methods 25*, 78−86.
54. Deniz, A. A., Laurence, T. A., Dahan, M., Chemla, D. S., Schultz, P. G., and Weiss, S. (2001) Ratiometric Single-Molecule Studies of Freely Diffusing Biomolecules, *Annu. Rev. Phys. Chem. 52*, 233−253.
55. Stryer, L., and Haugland, R. P. (1967) Energy Transfer: A Spectroscopic Ruler, *Proc. Natl. Acad. Sci. U.S.A. 58*, 716−726.
56. van der Meer, B. W., Coker, G., and Chen, S.-Y. (1994) *Resonance Energy Transfer: Theory and Data*, VCH, New York.
57. Cognet, L., Harms, G. S., Blab, G. A., Lommerse, P. H. M., and Schmidt, T. (2000) Simultaneous Dual-Color and Dual-Polarization Imaging of Single Molecules, *Appl. Phys. Lett. 77*, 4052−4054.
58. Sabanayagam, C. R., Eid, J. S., and Meller, A. (2005) Using Fluorescence Resonance Energy Transfer to Measure Distances Along Individual DNA Molecules: Corrections Due to Nonideal Transfer, *J. Chem. Phys. 122*, 061103.
59. Laurence, T. A., Kong, X., Jager, M., and Weiss, S. (2005) Probing Structural Heterogeneities and Fluctuations of Nucleic Acids and Denatured Proteins, *Proc. Natl. Acad. Sci. U.S.A. 102*, 17348−17353.
60. Schuler, B. (2005) Single-Molecule Fluorescence Spectroscopy of Protein Folding, *ChemPhysChem 6*, 1206−1220.
61. Allen, M. W., Urbauer, R. J. B., Zaidi, A., Williams, T. D., Urbauer, J. L., and Johnson, C. K. (2004) Fluorescence Labeling, Purification and Immobilization of a Double Cysteine Mutant Calmodulin Fusion Protein for Single-Molecule Experiments, *Anal. Biochem. 325*, 273−284.
62. Eggeling, C., Widengren, J., Brand, L., Schaffer, J., Felekyan, S., and Seidel, C. A. M. (2006) Analysis of Photobleaching in Single-Molecule Multicolor Excitation and Foerster Resonance Energy Transfer Measurements, *J. Phys. Chem. A 110*, 2979−2995.
63. Slaughter, B. D., Allen, M. W., Unruh, J. R., Urbauer, R. J. B., and Johnson, C. K. (2004) Single-Molecule Resonance Energy Transfer and Fluorescence Correlation Spectroscopy of Calmodulin in Solution, *J. Phys. Chem. B 108*, 10388−10397.
64. Müller, B. K., Zaychikov, E., Brauchle, C., and Lamb, D. C. (2005) Pulsed Interleaved Excitation, *Biophys. J. 89*, 3508−3522.
65. Andrec, M., Levy, R. M., and Talaga, D. S. (2003) Direct Determination of Kinetic Rates from Single-Molecule Photon Arrival Trajectories Using Hidden Markov Models, *J. Phys. Chem. A 107*, 7454−7464.
66. Watkins, L. P., and Yang, H. (2004) Information Bounds and Optimal Analysis of Dynamic Single Molecule Measurements, *Biophys. J. 86*, 4015−4029.
67. McHale, K., Berglund, A. J., and Mabuchi, H. (2004) Bayesian Estimation for Species Identification in Single-Molecule Fluorescence Microscopy, *Biophys. J. 86*, 3409−3422.
68. Witkoskie, J. B., and Cao, J. (2004) Single Molecule Kinetics. II. Numerical Bayesian Approach, *J. Chem. Phys. 121*, 6373−6379.
69. Kou, S. C., Xie, X. S., and Liu, J. S. (2005) Bayesian Analysis of Single-Molecule Experimental Data, *Appl. Statist. 54*, 469−506.
70. McKinney, S. A., Joo, C., and Ha, T. (2006) Analysis of Single-Molecule FRET Trajectories Using Hidden Markov Modeling, *Biophys. J. 91*, 1941−1951.
71. Antonik, M., Felekyan, S., Gaiduk, A., and Seidel, C. A. (2006) Separating Structural Heterogeneities from Stochastic Variations in Fluorescence Resonance Energy Transfer Distributions Via Photon Distribution Analysis, *J. Phys. Chem. B 110*, 6970−8.
72. Ha, T., Laurence, T. A., Chemla, D. S., and Weiss, S. (1999) Polarization Spectroscopy of Single Fluorescent Molecules, *J. Phys. Chem. B 103*, 6839−6850.
73. Peterman, E. J., Sosa, H., and Moerner, W. E. (2004) Single-Molecule Fluorescence Spectroscopy and Microscopy of Biomolecular Motors, *Annu. Rev. Phys. Chem. 55*, 79−96.

74. Sosa, H., Peterman, E. J., Moerner, W. E., and Goldstein, L. S. (2001) Adp-Induced Rocking of the Kinesin Motor Domain Revealed by Single-Molecule Fluorescence Polarization Microscopy, *Nat. Struct. Biol. 8*, 540−544.
75. Osborn, K. D., Bartlett, R. K., Mandal, A., Zaidi, A., Urbauer, R. J. B., Urbauer, J. L., Galeva, N., Williams, T. D., and Johnson, C. K. (2004) Single-Molecule Dynamics Reveal an Altered Conformation for the Autoinhibitory Domain of Plasma-Membrane Ca^{2+}-ATPase Bound to Oxidatively Modified Calmodulin, *Biochemistry 43*, 12937−12944.
76. Osborn, K. D., Zaidi, A., Mandal, A., Urbauer, R. J. B., and Johnson, C. K. (2004) Single-Molecule Dynamics of the Calcium-Dependent Activation of Plasma-Membrane Ca^{2+}-ATPase by Calmodulin, *Biophys. J. 87*, 1892−1899.
77. Osborn, K. D., Zaidi, A., Urbauer, R. J. B., Michaelis, M. L., and Johnson, C. K. (2005) Single-Molecule Characterization of the Dynamics of Calmodulin Bound to Oxidatively Modified Plasma-Membrane Ca^{2+}-ATPase, *Biochemistry 44*, 11074−11081.
78. Chin, D., and Means, A. R. (2000) Calmodulin: A Prototypical Calcium Sensor, *Trends Cell Biol. 10*, 322−328.
79. Yap, K. L., and Ikura, M. (2004) Calmodulin, *Handb. Metalloproteins 3*, 447−458.
80. Nelson, M. R., and Chazin, W. J. (1998) Calmodulin as a Calcium Sensor, in *Calmodulin and Signal Transduction* (Van Eldik, L. J., and Watterson, D. M., Eds.) pp 17−64, Academic Press, San Diego.
81. Nelson, M. R., and Chazin, W. J. (1998) An Interaction-Based Analysis of Calcium-Induced Conformational Changes in Ca^{2+} Sensor Proteins, *Protein Sci. 7*, 270−282.
82. Zhang, M., Tanaka, T., and Ikura, M. (1995) Calcium-Induced Conformational Transition Revealed by the Solution Structure of Apo Calmodulin, *Nat. Struct. Biol. 2*, 758−767.
83. Carafoli, E. (2002) Calcium Signaling: A Tale for All Seasons, *Proc. Natl. Acad. Sci. U.S.A. 99*, 1115−1122.
84. Babu, Y. S., Sack, J. S., Greenhough, T. J., Bugg, C. E., Means, W. E., and Cook, W. J. (1985) Three-Dimensional Structure of Calmodulin, *Nature 315*, 37−40.
85. Chattopadhyaya, R., Meador, W. E., Means, A. R., and Quiocho, F. A. (1992) Calmodulin Structure Refined at 1.7 Å Resolution, *J. Mol. Biol. 228*, 1177−1192.
86. Kretsinger, R. H. (1992) The Linker of Calmodulin: To Helix or Not to Helix, *Cell Calcium 13*, 363−376.
87. Persechini, A., and Kretsinger, R. H. (1988) The Central Helix of Calmodulin Functions as a Flexible Tether, *J. Biol. Chem. 263*, 12175−12178.
88. Chou, J. J., Li, S., Klee, C. B., and Bax, A. (2001) Solution Structures of Ca^{2+}-Calmodulin Reveals Flexible Hand-Like Properties of Its Domains, *Nat. Struct. Biol. 8*, 990−996.
89. Fallon, J. L., and Quiocho, F. A. (2003) A Closed Compact Structure of Native Ca^{2+}-Calmodulin, *Structure 11*, 1303−1307.
90. Slaughter, B. D., Unruh, J. R., Allen, M. W., Bieber Urbauer, R. J., and Johnson, C. K. (2005) Conformational Substates of Calmodulin Revealed by Single-Pair Fluorescence Resonance Energy Transfer: Influence of Solution Conditions and Oxidative Modification, *Biochemistry 44*, 3694−3707.
91. Slaughter, B. D., Bieber-Urbauer, R. J., and Johnson, C. K. (2005) Single-Molecule Tracking of Sub-Millisecond Domain Motion in Calmodulin, *J. Phys. Chem. B 109*, 12658−12662.
92. Török, K., Tzortzopoulos, A., Grabarek, Z., Best, S. L., and Thorogate, R. (2001) Dual Effect of ATP in the Activation Mechanism of Brain Ca^{2+} Calmodulin-Dependent Protein Kinase II by Ca^{2+} Calmodulin, *Biochemistry 40*, 14878−14890.
93. Allen, M. W., Bieber Urbauer, R. J., and Johnson, C. K. (2004) Single-Molecule Assays of Calmodulin Target Binding Detected with a Calmodulin Energy-Transfer Construct, *Anal. Chem. 76*, 3630−3637.
94. Barbato, G., Ikura, M., Kay, L. E., Pastor, R. W., and Bax, A. (1992) Backbone Dynamics of Calmodulin Studied by ^{15}N Relaxation Using Inverse Detected Two-Dimensional NMR Spectroscopy: The Central Helix Is Flexible, *Biochemistry 31*, 5269−5278.
95. Kuboniwa, H., Tjandra, N., Grzesiek, S., Ren, H., Klee, C. B., and Bax, A. (1995) Solution Structure of Calcium-Free Calmodulin, *Nat. Struct. Biol. 2*, 768−776.
96. Masino, L., Martin, S. R., and Bayley, P. M. (2000) Ligand Binding and Thermodynamic Stability of a Multidomain Protein, Calmodulin, *Protein Sci. 9*, 1519−1529.
97. Pedigo, S., and Shea, M. A. (1995) Quantitative Endoproteinase Gluc Footprinting of Cooperative Ca^{2+} Binding to Calmodulin: Proteolytic Susceptibility of E31 and E87 Indicates Interdomain Interactions, *Biochemistry 34*, 1179−1196.
98. Biekofsky, R. R., Martin, S. R., McCormick, J. E., Masino, L., Fefeu, S., Bayley, P. M., and Feeney, J. (2002) Thermal Stability of Calmodulin and Mutants Studied by (1)H-(15)N HSQC NMR Measurements of Selectively Labeled [(15)N]Ile Proteins, *Biochemistry 41*, 6850−6859.
99. Slaughter, B. D., Unruh, J. R., Price, E. S., Huynh, J. L., Bieber Urbauer, R. J., and Johnson, C. K. (2005) Sampling Unfolding Intermediates in Calmodulin by Single-Molecule Spectroscopy, *J. Am. Chem. Soc. 127*, 12107−12114.
100. Zagrovic, B., Snow, C. D., Khaliq, S., Shirts, M. R., and Pande, V. S. (2002) Native-Like Mean Structure in the Unfolded Ensemble of Small Proteins, *J. Mol. Biol. 323*, 153−164.
101. Fitzkee, N. C., and Rose, G. D. (2004) Reassessing Random-Coil Statistics in Unfolded Proteins, *Proc. Natl. Acad. Sci. U.S.A. 101*, 12497−12502.
102. Millett, I. S., Doniach, S., and Plaxco, K. W. (2002) Toward a Taxonomy of the Denatured State: Small Angle Scattering Studies of Unfolded Proteins, *Adv. Protein Chem. 62*, 241−262.
103. Tan, X., Hu, D., Squier, T. C., and Lu, H. P. (2004) Probing Nanosecond Protein Motions of Calmodulin by Single-Molecule Fluorescence Anisotropy, *Appl. Phys. Lett. 85*, 2420−2422.
104. Frauenfelder, H., Sligar, S. G., and Wolynes, P. G. (1991) The Energy Landscapes and Motions of Proteins, *Science 254*, 1598−1603.
105. Eisenmesser, E. Z., Bosco, D. A., Akke, M., and Kern, D. (2002) Enzyme Dynamics During Catalysis, *Science 295*, 1520−1523.
106. Widengren, J., Mets, U., and Rigler, R. (1995) Fluorescence Correlation Spectroscopy of Triplet States in Solution: A Theoretical and Experimental Study, *J. Phys. Chem. 99*, 13368−13379.
107. Palmer, A. G., 3rd, and Thompson, N. L. (1987) Theory of Sample Translation in Fluorescence Correlation Spectroscopy, *Biophys. J. 51*, 339−343.
108. Eggeling, C., Kask, P., Winkler, D., and Jager, S. (2005) Rapid Analysis of Forster Resonance Energy Transfer by Two-Color Global Fluorescence Correlation Spectroscopy: Trypsin Proteinase Reaction, *Biophys. J. 89*, 605−618.
109. Johnson, C. K., Slaughter, B. D., Unruh, J. R., and Price, E. S. (2006) Fluorescence Probes of Protein Dynamics and Conformations in Freely Diffusing Molecules. Single-Molecule Resonance Energy Transfer and Time-Resolved Fluorescence Methods, in *Reviews in Fluorescence* (Geddes, C. D., and Lakowicz, J. R., Eds.) Vol. 3, pp 239−259, Springer, New York.
110. Yap, K. L., Kim, J., Truong, K., Sherman, M., Yuan, T., and Ikura, M. (2000) Calmodulin Target Database, *J. Struct. Funct. Genomics 1*, 8−14.
111. Kasturi, R., Vasulka, C., and Johnson, J. D. (1993) Ca^{2+}, Caldesmon, and Myosin Light Chain Kinase Exchange with Calmodulin, *J. Biol. Chem. 268*, 7958−7964.
112. Persechini, A., White, H. D., and Gansz, K. J. (1996) Different Mechanisms for Ca^{2+} Dissociation from Complexes of Calmodulin with Nitric Oxide Synthase or Myosin Light Chain Kinase, *J. Biol. Chem. 271*, 62−67.
113. Penheiter, A. R., Filoteo, A. G., Penniston, J. T., and Caride, A. J. (2005) Kinetic Analysis of the Calmodulin-Binding Region of the Plasma Membrane Calcium Pump Isoform 4b, *Biochemistry 44*, 2009−2020.
114. Brasselet, S., Peterman, E. J. G., and Moerner, W. E. (2000) Single-Molecule Fluorescence Resonant Energy Transfer in Calcium Concentration Dependent Cameleon, *J. Phys. Chem. B 104*, 3676−3682.
115. Tang, J., Mei, E., Green, C., Kaplan, J., DeGrado, W. F., Smith, A. B., and Hochstrasser, R. M. (2004) Probing Structural Dynamics of Individual Calmodulin:Peptide Complexes in Hydrogels by Single-Molecule Confocal Microscopy, *J. Phys. Chem. B 108*, 15910−15918.
116. Liu, R., Hu, D., Tan, X., and Lu, H. P. (2006) Revealing Two-State Protein-Protein Interactions of Calmodulin by Single-Molecule Spectroscopy, *J. Am. Chem. Soc. 128*, 10034−10042.
117. Enyedi, A., Vorherr, T., James, P., McCormick, D. J., Filoteo, A. G., Carafoli, E., and Penniston, J. T. (1989) The Calmodulin Binding Domain of the Plasma Membrane Ca^{2+} Pump Interacts Both with Calmodulin and with Another Part of the Pump, *J. Biol. Chem. 264*, 12313−12321.
118. Slaughter, B. D. (2005) *Single-Molecule Studies of Calmodulin Conformation, Dynamics, and Folding*, Ph.D. Dissertation, University of Kansas, Lawrence, KS.

119. Carafoli, E. (1987) Intracellular Calcium Homeostasis, *Annu. Rev. Biochem. 56*, 395−433.
120. Penniston, J. T., and Enyedi, A. (1998) Modulation of the Plasma Membrane Ca^{2+} Pump, *J. Membr. Biol. 165*, 101−109.
121. Verma, A. K., Filoteo, A. G., Stanford, D. R., Wieben, E. D., Penniston, J. T., Strehler, E. E., Fischer, R., Heim, R., Vogel, G., Mathews, S., Strehler-Page, M.-A., James, P., Vorherr, T., Krebs, J., and Carafoli, E. (1988) Complete Primary Structure of a Human Plasma Membrane Ca^{2+} Pump, *J. Biol. Chem. 263*, 14152−14159.
122. Penheiter, A. R., Bajzer, Z., Filoteo, A. G., Thorogate, R., Török, K., and Caride, A. J. (2003) A Model for the Activation of Plasma Membrane Calcium Pump Isoform 4b by Calmodulin, *Biochemistry 42*, 12115−12124.
123. Toyoshima, C., Nomura, H., and Tsuda, T. (2004) Lumenal Gating Mechanism Revealed in Calcium Pump Crystal Structures with Phosphate Analogues, *Nature 432*, 361−368.
124. Xu, C., Rice, W. J., He, W., and Stokes, D. L. (2002) A Structural Model for the Catalytic Cycle of Ca^{2+}-ATPase, *J. Mol. Biol. 316*, 201−211.
125. Zaidi, A., Barron, L., Sharov, V. S., Schoneich, C., Michaelis, E. K., and Michaelis, M. L. (2003) Oxidative Inactivation of Purified Plasma Membrane Ca^{2+}-ATPase by Hydrogen Peroxide and Protection by Calmodulin, *Biochemistry 42*, 12001−12010.
126. Gao, J., Yao, Y., and Squier, T. C. (2001) Oxidatively Modified Calmodulin Binds to the Plasma Membrane Ca-ATPase in a Nonproductive and Conformationally Disordered Complex, *Biophys. J. 80*, 1791−1801.
127. Babu, Y. S., Bugg, C. E., and Cook, W. J. (1988) Structure of Calmodulin Refined at 2.2 Å Resolution, *J. Mol. Biol. 204*, 191−204.
128. Humphrey, W., Dalke, A., and Schulten, K. (1996) VMD: Visual Molecular Dynamics, *J. Mol. Graphics 14*, 33−38.
129. Toyoshima, C., Nakasako, M., Nomura, H., and Ogawa, H. (2000) Crystal Structure of the Calcium Pump of Sarcoplasmic Reticulum at 2.6 Å Resolution, *Nature 405*, 647−655.
130. Lushington, G. H., Zaidi, A., and Michaelis, M. L. (2005) Theoretically Predicted Structures of Plasma Membrane Ca^{2+}-ATPase and Their Susceptibilities to Oxidation, *J. Mol. Graphics Modell. 24*, 175−185.

BI061058E